Probing the Neutron Star Equation of State with Gravitational Wave Detectors

Frederic A. Rasio and Joshua A. Faber

Department of Physics and Astronomy, Northwestern University, Evanston, IL 60208

ABSTRACT

Coalescing binary neutron stars (NS) are expected to be an important source of gravitational waves detectable by laser interferometers. We discuss recent theoretical work on the hydrodynamics of NS binary mergers and possible methods for determining the NS compactness ratio M/R and constraining the equation of state of dense nuclear matter using gravitational wave signals. One particularly simple and promising method is based on the properties of quasi-equilibrium binary NS sequences and does not require full hydrodynamic merger calculations.

Keywords: gravitational radiation, neutron stars

1. INTRODUCTION

Coalescing compact binaries containing two neutron stars (NS) are among the most important sources of gravitational waves (GW) for LIGO,[1] VIRGO,[2] and other laser interferometers. Should the inspiral of such a binary be detected, the frequency evolution of the GW signal will immediately yield the system's "chirp mass" $M_{\rm ch} \equiv \mu^{3/5}\mathcal{M}^{2/5}$, where μ and $\mathcal{M}$ are the reduced and total mass of the binary, respectively. Higher-order post-Newtonian effects on the phase evolution of the signal also allow for the determination of the reduced mass μ, and thus the individual masses M_1 and M_2 of the two NS.[3] The determination of the NS radii in addition to their masses would yield important information about the equation of state (EOS) at nuclear densities, and could even indicate the presence of more exotic phases, such as strange quark matter instead of ordinary nuclear matter.[4] The GW signal of a coalescing binary could yield such information but this is limited in two different ways. During the slow inspiral phase at large separations, i.e., low frequencies ($f \ll 1\,$kHz), the stars behave like point masses, and finite-size effects are not expected to leave any signature in the GW signal.[3,5,6] During the final hydrodynamic merger, characteristic frequencies of GW emission could yield important information about the fluid EOS,[7,8,10] but these frequencies are expected to lie well above the photon shot noise limit of current interferometers (around 1 kHz). Thus, it is only during the last few orbits of the inspiral, just prior to merger, that we can hope to see the imprint of the NS radii on a measurable GW signal (below $\sim 1\,$kHz).

Several groups have studied this terminal phase of inspiral by constructing quasi-equilibrium sequences of close NS binaries in the conformal flatness approximation of general relativity (GR).[11–14] In this approximation, it is assumed that the binary system evolves along a sequence of appropriately constructed equilibrium states with decreasing binary separation as energy is radiated away in GW. From the binary equilibrium energy curve $E_{\rm eq}(r)$, which gives the total system energy as a function of binary separation r, and the GW luminosity $L_{\rm GW}$, one can derive the radial infall rate as $v_r = L_{\rm GW}(dE_{\rm eq}/dr)^{-1}$. With $v_r = dr/dt$ known, this provides the time evolution along the equilibrium sequence and the GW signal $h(t)$. This approach should remain accurate as long as the radial infall timescale r/v_r is longer than the dynamical timescale of the system, i.e., until the point where dynamical instability sets in, and the two stars plunge inward rapidly and merge.

Unfortunately, calculating the correct GW luminosity for a given matter configuration in GR is an extremely difficult task. Different approaches have required either time integration of the full non-linear equations of GR,[15] or the solution of a complicated wave equation for terms representing the spherical harmonic expansion of the GW metric perturbation.[16] The great complexity of these approaches is in stark contrast with the simplicity of the quasi-equilibrium approximation. However, we have recently shown[42] that the GW *energy spectrum* $dE_{\rm GW}/df$ can be calculated directly and very simply from the equilibrium energy curve, independent of any knowledge about the GW luminosity. Indeed, by definition of the quasi-equilibrium approximation, the energy

Gravitational-Wave Detection, Mike Cruise, Peter Saulson, Editors, Proceedings of SPIE
Vol. 4856 (2003) © 2003 SPIE · 0277-786X/03/$15.00

decrease $-dE_{\rm eq}$ between two neighboring binary configurations along the sequence is equal to the energy $dE_{\rm GW}$ radiated away as the wave frequency sweeps up by df, where the GW frequency is twice the orbital frequency, $f = 2f_{\rm orb}$. Thus, one should simply compute the total energy $E_{\rm eq}$ as a function of frequency f along the equilibrium sequence, and the GW energy spectrum is then given by the derivative $dE_{\rm GW}/df = -dE_{\rm eq}/df$. As a trivial example, consider the inspiral of two point masses in the Newtonian limit, where we have $E_{\rm eq} \propto -r^{-1}$ and $f \propto r^{-3/2}$. It follows that $E_{\rm eq} \propto -f^{2/3}$ and thus $dE_{\rm GW}/df \propto f^{-1/3}$, a well-known result. In addition to the assumptions underlying the quasi-equilibrium approximation, the validity of this simple approach relies on the additional assumption that the GW emission during the later merger phase has no effect on the energy spectrum at lower frequencies. Indeed, this has been demonstrated in numerical hydrodynamic calculations of binary mergers,[7,8] which show a clear separation between the inspiral and merger components of the emission in frequency space (see Sec. 3 below).

2. ENERGY SPECTRA IN THE QUASI-EQUILIBRIUM APPROXIMATION

We have investigated the properties of the GW emission during the final phase of binary NS inspiral using new, highly accurate equilibrium sequences calculated with the Meudon code.[17] The formalism is based on the conformally flat approximation, which is expected to yield accurate equilibrium matter configurations for this phase.[11–14] The resulting five non-linear, coupled elliptic equations are solved using a multi-domain spectral method.[18,19] This approach has already been used successfully in various astrophysical applications.[14,20,21] Typically, the computed fields satisfy the constraints of full GR to within $\sim 1\%$.[22] The code has been improved recently, especially with regard to the treatment of the external compactified domain, and the numerical error in computing equilibrium configurations, measured in terms of how well the virial theorem is satisfied, is of order one part in 10^5. The equilibrium sequences presented here are the natural extension of the work already published in Refs. 14 and 23, and are discussed in more detail in Ref. 24. Here we only show the variation of the ADM mass of the system (total binary mass-energy $\mathcal{M} \equiv c^{-2}E_{\rm eq}$) and the GW frequency (twice the orbital frequency), which are sufficient for our purposes to determine the GW energy spectrum.

The equilibrium configurations have been calculated for irrotational binaries, i.e., assuming that the fluid has zero vorticity in the inertial frame. Indeed, the NS should be spinning slowly at large separations and the viscosity of NS matter is too small for tidal spin-up to become significant on the coalescence timescale.[5,25] Based on the current set of well-measured NS masses in relativistic binary radio pulsars, it is expected that all NS in coalescing binaries will have masses $M \simeq 1.35 M_\odot$.[26] Hence, for simplicity, we consider only equal-mass binaries where $M_1 = M_2 = 1.35 M_\odot$. Also for simplicity, we model the NS EOS with a simple polytropic form $P = K\rho^\Gamma$, where P is the pressure and ρ the rest-mass density. The constant K represents the overall compressibility of the matter and largely sets the value of the stellar radius for a given mass, while the adiabatic exponent Γ measures the stiffness of the EOS and affects the degree of central concentration of the NS interior. Based on our experience with hydrodynamic calculations,[8,9] we expect that the GW energy spectrum just prior to merger is determined primarily by the NS radius through K, with relatively little sensitivity to Γ. For this reason, in this initial study, we allow K, and therefore also the stellar radius R, to vary for different NS models, but we set $\Gamma = 2$ for all models, as this value fits well most published NS EOS (see, e.g., Ref. 27 and references therein). Specifically, we consider NS models with compactness ratios $M/R = 0.12$, 0.14, 0.16, and 0.18 (setting $G = c = 1$), where M is the ADM (gravitational) mass measured by an observer at infinity for a single isolated NS, and R is the circumferential radius of the NS. For $M = 1.35\,M_\odot$, the corresponding radii are $R = 16.6$, 14.2, 12.4, and 11.1 km, respectively, spanning the range of values for NS radii calculated from various physical EOS. Note, however, that our results are unchanged under the rescaling given by $R' = \kappa R$, $M' = \kappa M$, $f' = f/\kappa$, for any constant κ.

For each NS model, about 12 binary equilibrium configurations have been computed with decreasing separations, until a cusp develops on the NS surface. Equilibrium configurations for smaller separations do not exist. To each sequence we fit a curve of the form

$$\mathcal{M}(f) = 2.7 M_\odot - k_{\rm N} f^{2/3} + k_1 f + k_2 f^2 \qquad (1)$$

to represent the variation of total mass-energy as a function of GW frequency. The first term gives the total gravitational mass of the system at infinite separation, while the second term represents the Newtonian point-mass behavior, with $k_{\rm N} = 2^{-4/3}\pi^{2/3}G^{2/3}M^{5/3} = 4.056 \times 10^{-4}\,M_\odot\,{\rm Hz}^{-2/3}$. The term $\propto f$ was introduced heuristically to represent the lowest-order post-Newtonian and finite-size corrections to the point-mass behavior at intermediate frequencies. The term $\propto f^2$ represents the tidal interaction energy, which causes the equilibrium energy curve to flatten at high frequencies.

Our best (least-squares) fit values of k_1 and k_2 for each sequence are listed in Table 1 and the results are illustrated in Fig. 1. The asterisks show the data points along each sequence, with a typical error between the data points and the fit of $\delta\mathcal{M} \sim 10^{-4}\,M_\odot$. We find in all cases that k_2 is positive, as we would expect: tidal deformations and relativistic gravitational effects increase the equilibrium energy.[28,29] We note that none of the equilibrium curves shows evidence of an energy minimum, which would have implied the onset of dynamical instability.[6,23,28,30]

Our choice of a heuristic fitting function, rather than one grounded in standard post-Newtonian (PN) theory, represents the best fit to the data we could achieve, using as few free parameters as possible. As such, we find it necessary to refrain from interpreting our fitting coefficients in terms of classical PN effects. It is possible to switch to a 1PN+2PN fitting formula (i.e., using terms with frequency dependence $f^{4/3}$ and f^2, rather than f and f^2), but the results presented here would remain essentially unchanged. In any case, the strength of our method is that it should work regardless of the fitting formula. All we require to create an energy spectrum is the derivative of the equilibrium energy as a function of frequency. Ideally, the energy spectrum could be computed by finite differencing from an equilibrium sequence whose points were calculated at sufficiently small spacing as to allow the required numerical accuracy.

Computing the GW energy spectrum for each model only requires differentiating the fitted curves with respect to frequency. The results are shown in Fig. 2. In each case, we see a characteristic frequency range where the spectrum plunges rapidly below the extrapolation of the point-mass (low-frequency) result. This corresponds to the flattening of the energy curves in response to the growing tidal deformation of each NS. Also shown is the energy spectrum of a 3PN, irrotational, point-mass binary, computed according to the results found in Ref. 31, which closely tracks our most compact model, indicating that the differences we see in the energy spectra result from finite-size effects associated with the NS radius. As the formula for the 3PN curve can be calculated analytically, the energy spectrum was computed by finite differencing, rather than fitting to a specified functional form. To quantify the deviations from the Newtonian case, seen in both the PN and conformally flat sequences, we define a set of break frequencies, at which the energy spectrum has dropped by some factor below the point-mass result. The values we find for f_{10}, f_{25}, and f_{50}, where $dE_{\rm GW}/df$ has dropped by 10%, 25%, and 50%, respectively, are listed in the last three columns of Table 1. We see that all these characteristic frequencies lie within the frequency range accessible by LIGO-type detectors, with perhaps the exception of f_{50} for the more compact sequences. Note that the calculation of f_{50} values requires extrapolating the equilibrium energy curves slightly beyond the last equilibrium model (where a cusp develops), and may therefore be less reliable. However, we find that f_{50} has a particularly steep, quasi-linear dependence on the NS compactness, given by $f_{50} \simeq [10^4(M/R) - 460]\,{\rm Hz}$ within the range of NS radii we considered. For comparison, f_{25} values can be determined safely within the quasi-equilibrium approximation, and the sensitivity on compactness is only slightly reduced, with $f_{25} \simeq [5000(M/R) - 85]\,{\rm Hz}$.

The best definition of the break frequency will be a tradeoff between higher signal-to-noise ratio at lower frequencies,[32] and greater ease of discrimination between different EOS at the higher frequencies. In addition, the quasi-equilibrium approximation is expected to be most accurate at lower frequencies, where the inspiral rate is slower. However, we doubt that this could become a major issue: if we adopt, for simplicity, the point-mass formula for the GW luminosity, and compute the corresponding radial infall velocity along our equilibrium sequences, we find that v_r never exceeds 5% of the orbital velocity, even at the point where we define f_{50} (the corresponding fraction at the point where we define f_{25} is about 2%).[33] Ultimately, the optimum choice should be determined by experimenters, taking into account the accuracy with which the break frequencies can be extracted using matched filtering techniques.[3,34] Defining a precise break frequency may not even be necessary. Instead, we suggest that GW inspiral templates could be terminated at high frequency in a manner that reproduces the energy spectrum given by a simple analytic form, such as our Eq. (1). The free parameters

k_1 and k_2 could then be measured experimentally and compared directly to the predictions of various realistic EOS used in computing binary equilibrium sequences. In future work, we plan to compute such sequences, and the corresponding energy curves, for a wide variety of published, realistic NS EOS.

3. HYDRODYNAMIC CALCULATIONS OF BINARY MERGERS

Beyond the point where the quasi-equilibrium assumption breaks down, the GW energy spectrum can only be computed from a full hydrodynamic calculation of the binary NS coalescence. Two very different computational schemes have been used in these calculations. Starting with the first hydrodynamic calculations of binary NS mergers in Newtonian gravity,[35] some groups have used grid-based, Eulerian finite-difference codes to solve the field equations of the chosen gravitational formalism. Most recently, these codes have been used to calculate the evolution of merging binary NS in a completely consistent, fully GR formalism.[36] Alternatively, several groups have used the particle-based Lagrangian SPH technique,[37] solving the field equations either on grids or by tree-based methods. These calculations have been done most recently in PN gravity for a wide variety of systems,[8,38] and in the conformally flat approximation for initially synchronized binaries.[10]

The GW energy spectra predicted by full hydrodynamic calculations differ in two important ways from those computed from equilibrium sequences. First, they typically contain very sharp peaks of emission, representing the characteristic frequencies of GW emission during the merger itself as well as from the oscillations of the merger remnant ("ringdown"). Second, the characteristic frequencies of emission extend to much higher frequencies $f > 1\,\mathrm{kHz}$, outside of the current LIGO frequency window. To measure these signals, it will be necessary to use specially designed narrow-band instruments, most likely using the "dual recycling" techniques now being tested at GEO 600.[39]

The GW energy spectrum from a PN hydrodynamic merger calculation can be computed from the two polarizations of the GW signal, $h_+(t)$ and $h_\times(t)$, following the techniques developed in Ref. 7. We first take the Fourier transforms of both polarizations of the GW signal,

$$\tilde{h}_+(f) = \int e^{2\pi i f t} h_+(t)\, dt, \tag{2}$$

$$\tilde{h}_\times(f) = \int e^{2\pi i f t} h_\times(t)\, dt, \tag{3}$$

and we insert them into the following expression giving the energy loss per unit frequency interval (see, e.g., Ref. 40),

$$\frac{dE}{df} = \frac{c^3}{G}\frac{\pi}{2}(4\pi r^2) f^2 \left\langle |\tilde{h}_+(f)|^2 + |\tilde{h}_\times(f)|^2 \right\rangle, \tag{4}$$

where the averages are taken over time as well as solid angle. In terms of the components of the quadrupole tensor, we then find

$$\begin{aligned} \frac{dE}{df} &= \frac{\pi^2 G}{c^5}\left[\frac{8}{15}\left(|\tilde{Q}^{(2)}_{xx} - \tilde{Q}^{(2)}_{yy}|^2 + |\tilde{Q}^{(2)}_{xx} - \tilde{Q}^{(2)}_{zz}|^2 + |\tilde{Q}^{(2)}_{yy} - \tilde{Q}^{(2)}_{zz}|^2\right) + \right. \\ &\left. \frac{48}{15}\left(|\tilde{Q}^{(2)}_{xx}|^2 + |\tilde{Q}^{(2)}_{yy}|^2 + |\tilde{Q}^{(2)}_{zz}|^2\right)\right], \end{aligned} \tag{5}$$

where $\tilde{Q}^{(2)}_{ij}$ represents the Fourier transform of the second derivative of the traceless quadrupole tensor.

Typical results, based on our own recent PN SPH calculations, are shown in Fig. 3. The initial binary in this calculation contains two identical NS with an EOS taken to be a $\Gamma = 3$ polytrope. More details about this and other similar calculations can be found in Ref. 9. In summary, relaxed initial SPH particle configurations for isolated NS in PN gravity were constructed, and linearly rescaled in three dimensions to correspond to the axis ratios determined by semi-analytical techniques for minimizing the energy of binary triaxial ellipsoids.[29] The evolution equations were evolved using a second-order leap-frog technique, with field equations (all of Poisson type) solved on a grid by an FFT-based convolution algorithm. The hydrodynamic equations were solved by

standard SPH techniques, involving interactions between particles determined by SPH smoothing kernels, whose smoothing lengths were allowed to vary in time to adjust to the local density.

The three labeled frequencies in the figure, $f_{\rm dyn}$, $f_{\rm peak}$, and $f_{\rm rem}$, correspond to the onset of dynamical instability, the emission during the merger itself, and the ringdown of the merger remnant, respectively. The dashed curve shows the energy spectrum derived exclusively from the signal taken from the dynamical calculation. The dotted curve represents a point-mass Newtonian inspiral, which is attached onto the beginning of the computed curve to minimize aliasing of the signal during the Fourier transform. As can be seen from the combined signal, shown as a solid curve, the two components tend to represent entirely different frequency regimes, with only minimal overlap in frequency space, corresponding to the initial GW frequency of the dynamical calculation. The characteristic frequencies highlighted in the figure are all important, and we turn our attention to each in turn.

At the highest frequencies, there is a very clear peak in the emission at $f_{\rm rem} \simeq 2000\,{\rm Hz}$, which results from GW emission by the merger remnant. This feature has been seen in all PN and conformally flat calculations, as well as those fully GR calculations which produce a central NS, rather than immediate collapse to a black hole.[41] The frequency this peak can tell us a great deal about the moment of inertia I of the merger remnant, and thus the NS EOS, as long as we make a few simplifying assumptions. If we assume that $f_{GW} = \Omega/\pi = J/I$, where J is the total angular momentum of the merger remnant and Ω its angular velocity, we can use our information about the system prior to merger to determine the values of the same parameters afterwards. The total angular momentum of the system immediately prior to merger decreases during the merger itself, with losses attributable to two completely different effects. First, we know that GW carry angular momentum from a system as well as energy. Typically, $5-10\%$ of the system angular momentum is carried off from the moment where the binary becomes dynamically unstable until the formation of the merger remnant signifying the end of the merger process. Second, the ejection of even a small amount of matter during the merger can carry off a great deal of angular momentum. However, hydrodynamic calculations have found that the amount of mass shed during the merger is extremely small whenever the NS are similar in mass. Calculations using all three gravitational schemes discussed previously typically find that less than 0.1% of the total system mass is ejected to infinity and that no more than a few percent of the total system mass is deposited in a low-density halo around the merger remnant. Using this information, as well as a measurement of the system mass from the inspiral component of the signal, we can estimate the total angular momentum of the merger remnant, and use the frequency of the merger remnant GW emission to derive a characteristic radius for the remnant and constrain the NS EOS. Unfortunately, as simple as this approach would be, it is limited by the incredibly difficult practical challenge of detecting a signal at these frequencies. The detectors which could measure this effect are at least a decade away, even according to the most optimistic estimates. It is more likely that the initial constraints on the NS radius and EOS will be drawn from features found at lower frequencies (as we discussed in Sec. 2 above).

The emission peak seen in Fig. 3 at $f_{\rm peak} \simeq 1500\,{\rm Hz}$ is closer to the frequency range where LIGO has good sensitivity, but the detection of such a feature presents several problems as well. First, there is a great uncertainty as to the width of such a feature, to the point where some results[9] show it as a peak in the energy spectrum, whereas others show either a plateau or even a slight drop.[10] Given these uncertainties, it is extremely difficult to devise a test which could pick these frequencies out of the data.

A more likely candidate for detection is the frequency at which dynamical stability sets in, labeled $f_{\rm dyn}$. As discussed in Sec. 2, we expect to see a drop in the energy spectrum corresponding to the growing dynamical instability of the binary system (even if such a system does not actually reach an energy minimum, as found in Newtonian and PN systems). The drop in the energy spectrum representing the onset of instability was seen in the original Newtonian work on the subject[7] as well as PN calculations.[9] It was not seen in calculations using a conformally flat gravitational formalism, but this may result from the use of a point-mass curve which does not replicate the correct Newtonian limit.[10]

This dip in the energy spectrum, which can be seen in dynamical calculations as well as those based on equilibrium sequences, is essentially the only feature which lies within the frequency range accessible to LIGO and other broad-band detectors. In fact, by comparing a dynamical calculation to an equilibrium sequence

calculation, it should be possible to determine the upper frequency limit below which the quasi-equilibrium approximation remains valid, as well as the behavior of the energy spectrum at frequencies just above this point.

ACKNOWLEDGMENTS

We are grateful to Philippe Grandclément and Keisuke Taniguchi for their help in constructing the quasi-equilibrium sequences of Sec. 2. This work was supported by NSF Grants PHY-0070918 and PHY-0133425.

REFERENCES

1. A. Abramovici *et al.*, Science **256**, 325 (1992); A. Abramovici *et al.*, Phys. Lett. A **218**, 157 (1996).
2. C. Bradaschia *et al.*, Nucl. Inst. Methods **A289**, 518 (1990); B. Caron *et al.*, Class. Quantum Grav. **14**, 1461 (1997).
3. C. Cutler and E.E. Flanagan, Phys. Rev. D **49**, 2658 (1994).
4. For a review of the topic, see K.S. Cheng, Z.G. Dai, and T. Lu, Int. J. Mod. Phys. D **7**, 139 (1998); J. Madsen, in *Hadrons in Dense Matter and Hadrosynthesis*, edited by J. Cleymans, H.B. Geyer, and F.G. Scholtz (New York, Springer, 1999), p. 162. For a discussion of systems which may contain quark stars, see P. Slane, D.J. Helfand, and S.S. Murray, Astrophys. J. Lett. **571**, L45 (2002); J.J. Drake *et al.*, Astrophys. J. **572**, 996 (2002); Astrophys. J., (2002); F.M. Walter and J. Lattimer, preprint, astro-ph/0204199 (2002).
5. C.S. Kochanek, Astrophys. J. **398**, 234 (1992).
6. D. Lai, F.A. Rasio, and S.L. Shapiro, Astrophys. J. Lett. **406**, L63 (1993).
7. X. Zhuge, J.M. Centrella, and S.L.W. McMillan, Phys. Rev. D **50**, 6247 (1994); **54**, 7261 (1996).
8. J.A. Faber and F.A. Rasio, Phys. Rev. D **62**, 064012 (2000); J.A. Faber, F.A. Rasio, and J.B. Manor, *ibid.* **63**, 044012 (2001).
9. J.A. Faber and F.A. Rasio, Phys. Rev. D **65**, 084042 (2002).
10. R. Oechslin, S. Rosswog, and F.-K. Thielemann, Phys. Rev. D **65**, 103005 (2002).
11. T.W. Baumgarte *et al.*, Phys. Rev. Lett. **79**, 1182 (1997); Phys. Rev. D **57**, 7299 (1998).
12. P. Marronetti, G.J. Mathews and J.R. Wilson, Phys. Rev. D **60**, 087301 (1999).
13. K. Uryu, and Y. Eriguchi, Phys. Rev. D **61**, 124023 (2000).
14. E. Gourgoulhon *et al.*, Phys. Rev. D. **63**, 064029 (2001).
15. M.D. Duez, T.W. Baumgarte, and S.L. Shapiro, Phys. Rev. D **63**, 084030 (2001); M.D. Duez *et al.*, *ibid.* **65**, 024016 (2002).
16. M. Shibata and K. Uryu, Phys. Rev. D **64**, 104017 (2001).
17. The code is publicly available, see `http://www.lorene.obspm.fr` for more details.
18. S. Bonazzola and J.-A. Marck, J. Comp. Phys. **87**, 201 (1990); S. Bonazzola, E. Gourgoulhon and J.-A. Marck, Phys. Rev. D **58**, 104020 (1998).
19. P. Grandclément *et al.*, J. Comp. Phys. **170**, 231 (2001).
20. E. Gourgoulhon *et al.*, Astron. Astrophys. **349**, 851 (1999).
21. P. Grandclément, E. Gourgoulhon and S. Bonazzola, Phys. Rev. D **65**, 044021 (2002).
22. G.J. Mathews, P. Marronetti and J.R. Wilson, Phys. Rev. D **58**, 043003 (1998).
23. K. Taniguchi, E. Gourgoulhon and S. Bonazzola, Phys. Rev. D **64**, 064012 (2001); K. Taniguchi and E. Gourgoulhon, Phys. Rev. D **65**, 044027 (2002).
24. K. Taniguchi and E. Gourgoulhon, preprint, gr-qc/0207098 (2002).
25. L. Bildsten and C. Cutler, Astrophys. J. **400**, 175 (1992).
26. S.E. Thorsett and D. Chakrabarty, D., Astrophys. J. **512**, 288 (1999).
27. J.M. Lattimer and M. Prakash, Astrophys. J. **550**, 426 (2001).
28. D. Lai, F.A. Rasio, and S.L. Shapiro, Astrophys. J. **420**, 811 (1994).
29. J.C. Lombardi, F.A. Rasio, and S.L. Shapiro, Phys. Rev. D **56**, 3416 (1997).
30. D. Lai, F.A. Rasio, and S.L. Shapiro, Astrophys. J. Suppl. **88**, 205 (1993).

31. T. Damour, P. Jaranowski, and G. Schäfer, Phys. Rev. D **62**, 044024 (2000); **62**, 084011 (2000).
32. The peak sensitivity of the initial LIGO detectors will be around 150 Hz (see Ref.[1]), while for more advanced detectors it could be as high as 500 Hz, see E. Gustafson, D. Shoemaker, K. Strain, and R. Weiss, LIGO White Paper T990080-00-D, 1999 (unpublished); The report is available from `http://www.ligo.caltech.edu/docs/T/T990080-00.pdf`
33. Even when finite-size effects are taken into account in full GR calculations, the radial infall velocity still does not exceed about 15% of the orbital velocity at any point along the equilibrium sequence for an assumed compactness of $M/R = 0.19$, and for a compactness $M/R = 0.14$, the ratio never exceeds 5%; see Fig. 15 of Ref..[16]
34. E.E. Flanagan and S.A. Hughes, Phys. Rev. D **57**, 4535 (1998); **57**, 4566 (1998).
35. K. Oohara and T. Nakamura, Prog. Theor. Phys. **82**, 535 (1989); T. Nakamura and K. Oohara, *ibid.* **82**, 1066 (1989); K. Oohara and T. Nakamura, *ibid.* **83**, 906 (1990); T. Nakamura and K. Oohara, *ibid.* **86**, 73 (1991).
36. M. Shibata and K. Uryu, Prog. Theor. Phys. **107**, 265 (2002).
37. See, e.g., F.A. Rasio and S.L. Shapiro, Astrophys. J. **401**, 226 (1992), and references therein for a description of the method.
38. S. Ayal *et al.*, Astrophys. J. **550**, 846 (2001).
39. H. Lück *et al.*, Class. Quantum Grav. **14**, 1471 (1997); K. Danzmann, in *Relativistic Astrophysics*, proceedings of the 162nd W.E. Heraeus Seminar, edited by H. Riffert *et al.* (Wiesbaden: Vieweg Verlag, 1998), p.48.
40. K.S. Thorne, in *300 Years of Gravitation*, edited by S. Hawking and W. Israel (Cambridge University Press, 1987), p. 330.
41. For this, and the discussion which follows, all relevant results can be found in Refs. 9, 10, 36, and 38.
42. J.A. Faber, P. Grandclément, F.A. Rasio and K. Taniguchi, preprint gr-qc/0201040, submitted to PRL (2002).

Table 1. Properties of the quasi-equilibrium sequences. Here M/R (with $G = c = 1$) is the compactness of an isolated NS seen by an observer at infinity, R is the circumferential radius for an ADM mass of $M = 1.35\,M_\odot$, $f_{\rm c}$ is the GW frequency at the final point of each sequence (cusp), k_1 and k_2 are the best fit parameters in Eq. 1, and f_{10}, f_{25}, and f_{50} are the break frequencies at which the GW energy spectrum has dropped, respectively, by 10%, 25%, and 50% below the point-mass energy spectrum.

M/R	R (km)	$f_{\rm c}$ (Hz)	k_1	k_2	f_{10} (Hz)	f_{25} (Hz)	f_{50} (Hz)
0.12	16.6	641	-4.939E-6	1.290E-8	342	518	764
0.14	14.2	807	-3.363E-6	9.244E-9	383	612	931
0.16	12.4	1002	-1.806E-6	6.490E-9	418	720	1137
0.18	11.1	1187	-5.834E-7	4.835E-9	431	810	1331

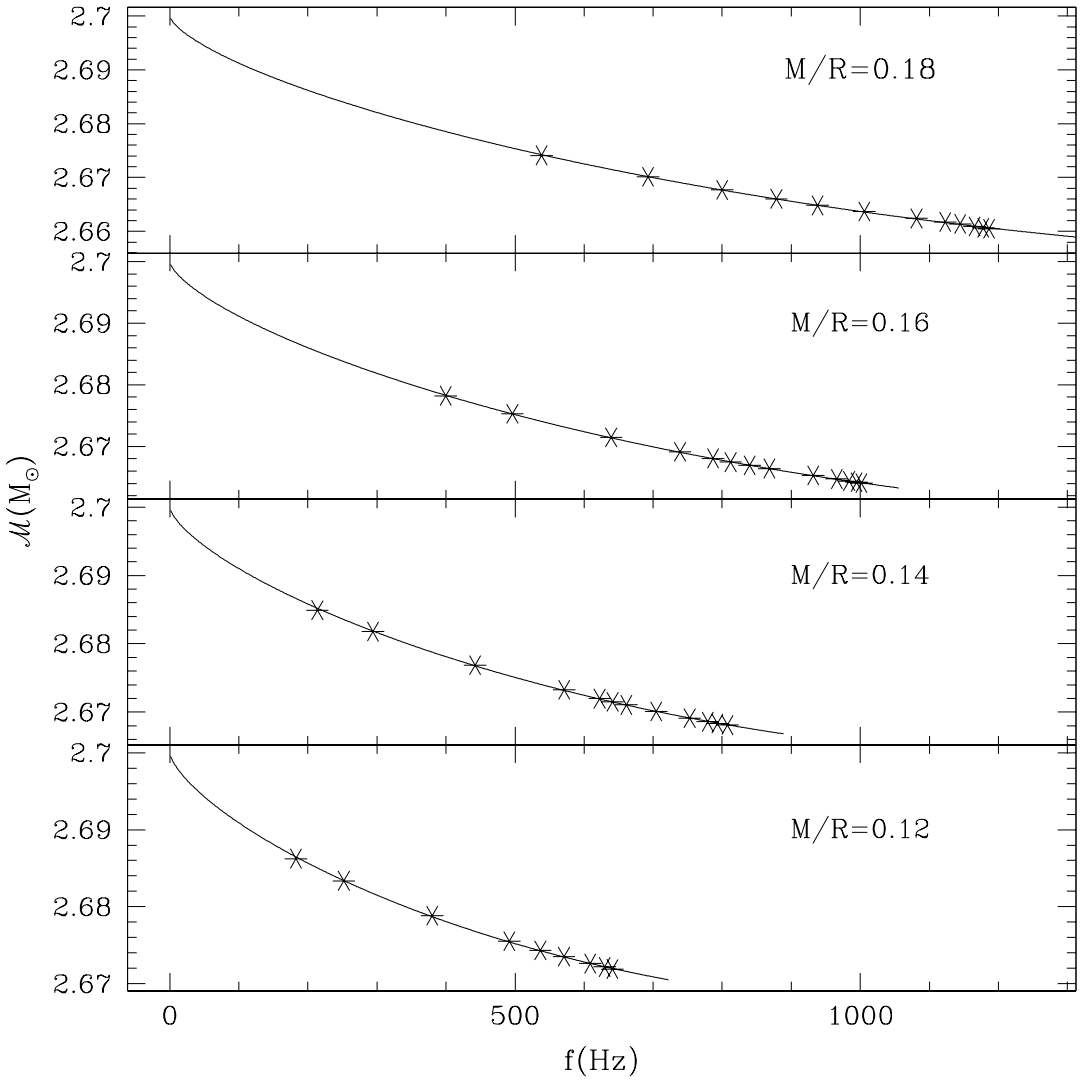

Figure 1. ADM mass (total mass-energy) of a binary NS system as a function of GW frequency (twice the orbital frequency), computed along each of our 4 irrotational equilibrium sequences. From bottom to top, the sequences correspond to NS with compactness $M/R = 0.12, 0.14, 0.16$, and 0.18. All models assume a polytropic EOS with $\Gamma = 2$ and a NS mass of $1.35\,M_\odot$ for both components. The asterisks indicate the individual equilibrium configurations calculated along each sequence, while the lines show our best fit using Eq. (1) and the values of Table 1.

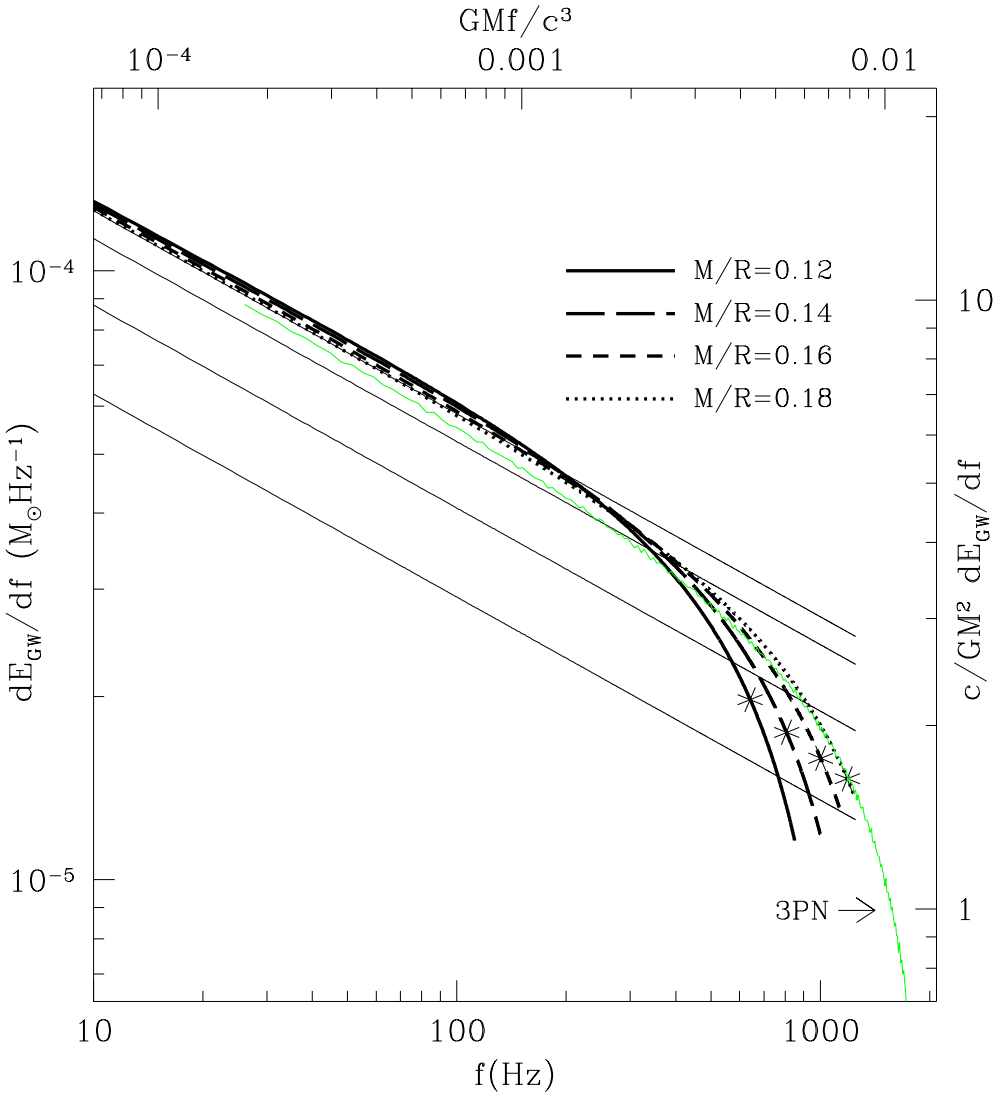

Figure 2. Energy spectrum $dE_{\rm GW}/df$ of GW emission emitted along each of the 4 sequences of Fig. 1 in the quasi-equilibrium approximation, as well as that for an irrotational 3PN point mass binary from Ref. 31, which closely tracks our most compact model. Asterisks indicate the terminal point along each sequence, where a cusp develops. The slanted straight lines show, from top to bottom, the point-mass Newtonian energy spectrum ($\propto f^{-1/3}$) multiplied by 1.0, 0.9, 0.75, and 0.5. The last three values are used to define characteristic break frequencies f_{10}, f_{25}, and f_{50}, where the energy spectrum has dropped by the corresponding fraction. The units on the right and top axes show the corresponding dimensionless quantities, with the mass dependence scaled away. Note that the 3PN curve, which can be calculated in a semi-analytic fashion, was computed by finite-differencing, rather than fitting a parameterized function.

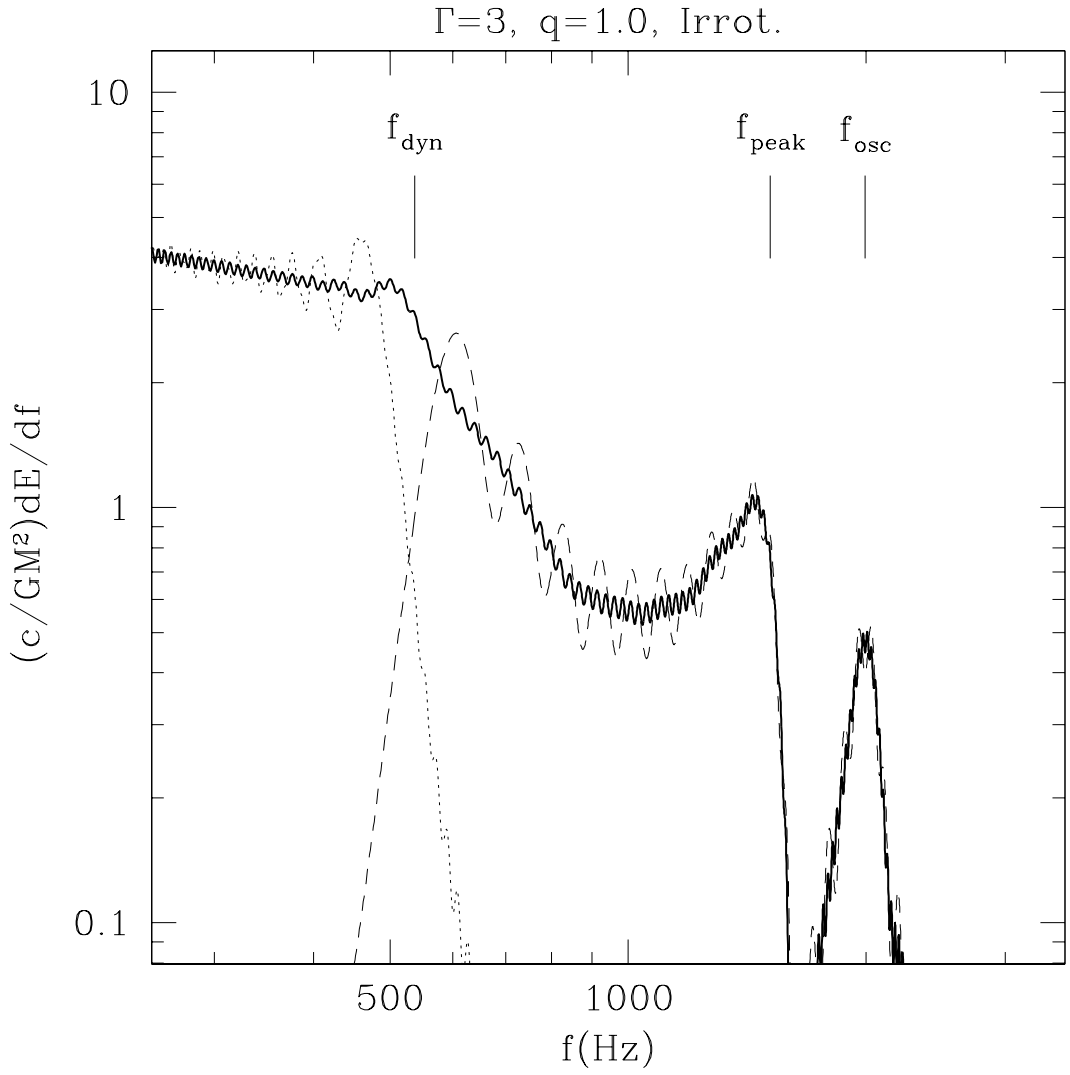

Figure 3. Energy spectrum from a typical PN SPH calculation of a NS binary merger with binary mass ratio $q = 1.0$, and assuming a simple polytropic NS EOS with $\Gamma = 3$ (from Ref. 31). We show the inspiral (dotted line) and merger (dashed line) subcomponents of the spectrum, as well as the total combined spectrum (heavy solid line). The labeled frequencies represent the characteristic GW frequency at the onset of dynamical instability ($f_{\rm dyn}$), during the merger itself when the GW luminosity peaks ($f_{\rm peak}$), and during the phase of merger remnant oscillations ($f_{\rm rem}$). The frequencies are given for a NS mass $M = 1.35 M_\odot$.